Aerial Additive Manufacturing with Multiple Autonomous Robots

Ketao Zhang[1,2], Pisak Chermprayong[1], Feng Xiao[1], Dimos Tzoumanikas[3], Barrie Dams[4], Sebastian Kay[5], Basaran Bahadir Kocer[1], Alec Burns[5], Lachlan Orr[1,8], Christopher Choi[3], Durgesh Dattatray Darekar[5], Wenbin Li[3], Steven Hirschmann[5], Valentina Soana[5], Shamsiah Awang Ngah[4], Sina Sareh[1], Ashutosh Choubey[1], Laura Margheri[1], Vijay M. Pawar[5], Richard J. Ball[4], Chris Williams[4], Paul Shepherd[4], Stefan Leutenegger[3,6], Robert Stuart-Smith[5,7] & Mirko Kovac[1,8]*

[1] *Department of Aeronautics, Imperial College London, South Kensington Campus, London SW7 2AZ, UK.*

[2] *School of Engineering and Materials Science, Queen Mary University of London, Mile End Road, London E1 4NS, UK.*

[3] *Department of Computing, Imperial College London, South Kensington Campus, London SW7 2AZ, UK.*

[4] *Department of Architecture and Civil Engineering, University of Bath, Bath BA2 7AY, UK.*

[5] *Department of Computer Science, University College London, London WC1E 6BT, UK.*

[6] *Department of Informatics, Technical University of Munich, 85748 Garching, Germany.*

[7] *Stuart Weitzman School of Design, University of Pennsylvania, Philadelphia, PA 19104, USA.*

[8] *Materials and Technology Centre of Robotics, Swiss Federal Laboratories for Materials Science and Technology (Empa), 8600 Dübendorf, Switzerland.*

Additive manufacturing methods [1–4] using static and mobile robots are being developed for both on-site construction [5–8] and off-site prefabrication [9,10]. Here we introduce a new method of additive manufacturing, referred to as Aerial Additive Manufacturing (Aerial-AM), that utilizes a team of aerial robots inspired by natural builders [11] such as wasps who use collective building methods [12,13]. We present a scalable multi-robot 3D printing and path planning framework that enables robot tasks and population size to be adapted to variations in print geometry throughout a building mission. The multi-robot manufacturing framework allows for autonomous 3D printing under human supervision, real-time assessment of printed geometry and robot behavioural adaptation. To validate autonomous Aerial-AM based on the framework, we develop BuilDrones for depositing materials during flight and ScanDrones for measuring print quality, and integrate a generic real-time model-predictive-control scheme with the Aerial-AM robots. In addition, we integrate a dynamically self-aligning delta manipulator with the BuilDrone to further improve manufacturing accuracy to 5mm for printing geometry with precise trajectory requirements, and develop four cementitious-polymeric composite mixtures suitable for continuous material deposition. We demonstrate proof-of-concept prints including a cylinder of 2.05m with a rapid curing insulation foam material and a cylinder of 0.18m with structural pseudoplastic cementitious material, a light-trail virtual print of a dome-like geometry, and multi-robot simulations. Aerial-AM allows manufacturing in-flight

and offers future possibilities for building in unbounded, at height, or hard to access locations.

To deliver improvements in productivity and safety, robotics-based technologies for construction activities [14,15] have been developed for both the assembly of building elements [16–20] and free-form continuous additive manufacturing (AM) [1–4]. Compared to the assembly-based approaches, free-form continuous AM enables flexible production of geometrically variable designs that can provide improvements in material efficiency and cost reductions. Currently, approaches to large-scale free-form AM for on-site construction primarily utilise ground-based robots and gantry/crane systems [10]. These technologies, however, necessitate scaling-up robot hardware to a larger dimension than the desired print geometry's work envelope, rendering parallel operation or occupation of a building site by people or other machinery difficult and dangerous. Furthermore, these large-scale systems require a tethered connection to a power supply, limiting abilities to adapt to agile applications such as inspection/maintenance [21], repair [22], or manufacture in remote, hard to access, or hostile, environments [23], where transport or installation of large infrastructure is not feasible.

As an alternative approach to large single-robot systems, a team of small mobile robots could offer greater flexibility and scalability to build geometries larger in size than the individual robots themselves [24–27], and also have the potential to be adaptively distributed across several building sites efficiently and concurrently [13]. However, research into construction using a team of robots is at an early exploratory stage of development, and is to date, predominantly focused on the assembly of building elements. Further, the current multi-robot AM approaches mainly employ mobile ground robot-vehicles [7,8] that have limited operational height. These mobile systems are constrained to navigate either around or along the top of previously manufactured work [28], limiting building to geometries and materials that support the weight and motion of the robot platform and render untethered operation or the ability of robots to pass each other or ascend/descend the manufactured geometry challenging and to date, unresolved. A comparison of state-of-the-art robot platforms developed for additive manufacturing in the building industry is illustrated in Fig. 1.

In contrast to current artificial robot systems and their inherent limitations, natural builders demonstrate significant degrees of scalability and adaptability in building their habitats, and many do so with the aid of flight and additive building approaches. For example, a Barn Swallow overcomes a limited material payload by making twelve hundred trips between its material source and the construction site to incrementally complete its nest [29]. Social insects such as termites and wasps exhibit greater degrees of adaptability and scalability, especially the aerial construction undertaken by social wasps evinces efficient and direct path optimization, with flight alleviating the requirement to navigate over or around previously built material throughout the building process [12]. These natural systems inspired an approach to collective construction that employs a network of untethered mobile robots to operate as a multi-agent system [13]. Enlisting a large number of robots to work together reveals new challenges in manufacturing operations that require solutions to multi-agent coordination beyond currently available technologies. Along with collective interaction methods for the multi-robot system, material design and use, and environmental manipulation mechanisms must be integrated and co-developed to enable collective construction.

1 Aerial-AM Framework

Here, we report the first Aerial-AM framework, that couples the merits of natural precedents with engineering principles and enables additive manufacturing using unmanned aerial robots in-flight, demonstrating the untethered, unbounded three-dimensional printing system, and the first scalable swarm-based control system for distributed additive manufacturing by multiple aerial robots in parallel.

To achieve autonomous additive manufacturing with a team of aerial robots requires parallel development of a number of key enabling technologies, that include: 1) Aerial robots capable of high-accuracy material deposition and in-the-loop qualitative assessment of printing quality; 2) The ability for a team of aerial robots to broadcast their activities to one another, wirelessly sharing data independent of neighbor proximity; 3) Autonomous navigation and task planning systems to adaptively determine and distribute manufacturing tasks in conjunction with a printing path strategy; 4) Strategically engineered/selected materials, especially lightweight and printable cementitious mixes, suitable for the Aerial-AM approach without requiring formwork or temporary scaffolds.

Using the multi-disciplinary physical artificial intelligence (AI) development method [30], we developed the Aerial-AM system (Fig. 2, Supplementary Video 1) which employs two types of aerial robot platform referred to as BuilDrone and ScanDrone (Extended Data Fig. 1, Supplementary Method 1). The former was engineered to implement autonomous deposition of physical materials (Supplementary Methods 1, 2 and 3) with context-dependent manufacturing accuracy and the latter to perform incremental aerial scanning and validation observations (Supplementary Method 4) after material deposition of every layer. Both robot platforms were coordinated with a newly proposed distributed multi-agent approach (Supplementary Method 5) in two loops (Fig. 2a). The manufacturing strategy loop was developed to correlate the AM geometry and robot AM task allocation in a multi-agent system. The construction loop consists of in-flight printing performance characterization of both BuilDrones and ScanDrone, real-time trajectory adaptation and material extrusion by the BuilDrones and print verification through the ScanDrone and a human supervisor.

A multi-agent approach for Aerial-AM Aerial-AM requires a single or multiple untethered aerial robots to make coordinated autonomous flights to and from varying deposition locations. To enable operation within a large volume for building-scale manufacturing, this approach also requires local robot decision-making to adapt to external and dynamic parameters such as variations in task allocation, building geometry, external environment factors, resources and live concurrent activities during the act of building. To investigate the manufacturing performance of using this approach for coordinating multiple networked aerial robots, we present a Multi-Agent Aerial-AM framework (Supplementary Method 5) providing capabilities for live autonomous task allocation, spatial collision awareness, collective organisation and system robustness through redundancy (Supplementary Video 2).

Aerial-AM is designed to leverage bottom-up approaches to multi-robot control coupled with features for local sensing and mapping, enabling robots to operate autonomously with minimal supervision and providing systemic redundancy against problems such as loss of communication or robot mechanical failure. In developing the Aerial-AM framework, we evaluate the performance of a distributed approach to manufacturing and its adaption to building geometry at various scales.

Materials and printing paths In order to manufacture geometries at various scales using different materials, Aerial-AM process-related parameters such as printing path, printing head velocity, nozzle diameter and the accuracy of BuilDrones, had to be specified in conjunction with material properties whilst also considering the downwash from BuilDrone propellers. The ratio between the layer width and printing accuracy is the main factor considered in printing geometry design and path generation. Three scalable paths were designed for constructing cylindrical geometries - 1) multiple adjacent concentric circles effectively forming a solid wall, 2) a rounded Peano curve, with alternating layers staggered around the circle with a half-unit offset, and 3) A hybrid design with three non-adjacent concentric circles alternating with a rounded Peano curve (Extended Data Fig. 3). Informed by salient studies in AM construction cementitious [4,31–40] and foam materials [3,41,42] (Supplementary Method 6, Supplementary Tables 1 and 2), the development of Aerial-AM material strategies (Supplementary Method 6) focused on commercially available foams and specifically engineered cementitious pastes and mortars for Aerial-AM extrusion by BuilDrones. Control of fresh material rheology and curing times is important for formwork-free AM extrusion as, once deposited, fresh material required sufficient buildability to resist deformation due to self-weight and subsequent layers [43].

2 Demonstrations at Various Scales

Aerial-AM enables a team of aerial robots to manufacture in three dimensions, either in sequence or in parallel. To demonstrate the potential of this nature-inspired framework, we undertook three different experiments based on surfaces of revolution geometries at various scales.

Tall foam cylinder We first demonstrate the Aerial-AM approach by manufacturing a single contour wall of a cylindrical geometry with a constant diameter of 0.3 m (Fig. 3), which was chosen with consideration of the cross-section dimensions of a foam layer after expansion (Extended Data Fig. 1a). The cylinder was designed with a height of 2.05m, over 4 times the height of the BuilDrone itself to ensure the BuilDrone flew safely within the envelope of the testing space. The cylinder was printed by depositing low-density expanding foam with multiple trips by a BuilDrone, with scanning in-the-loop.

Here we use the rapid curing thermoplastic polyurethane foam to demonstrate proof of concept for Aerial-AM approach given the expanding foam material is suitable for both building insulation and form-work for in-situ cast-concrete structures [3]. Preliminary investigations revealed that rapid curing is essential to mitigate the deformation of fresh material due to downwash; therefore, a rapid-setting two-part foam system (density 30 kg/m^3) was used for BuilDrone extrusion (Supplementary Method 6).

Using the newly developed Model Predictive Control (MPC) schemes (Extended Data Fig. 4, Supplementary Method 3) for Aerial-AM robots, the foam printing BuilDrone was characterised and tuned to perform sufficient accuracy for depositing rapid-curing foam materials while implementing various flight trajectories. Preliminary printing tests showed that the layer height of printed foam material varies due to irregularities of material expansion though the BuilDrone performs accurate flight. To mitigate irregularities in the previous layer's deposition, we introduce the ScanDrone in the vision of in-the-loop qualitative assessment of printing quality to timely adjust the BuilDrone reference trajectory (Supplementary Video 3). The printing process of effective material deposition by BuilDrone took 29 minutes in the mission of completing the tall cylinder.

To evaluate the manufactured column geometry and obtain the adjustment of printing height, 3D geometric data were collected after every print layer autonomously with a ScanDrone using the mapping approach (Supplementary Method 4). Collected the depth images and poses by the motion tracking system, a state-of-the-art dense mapping algorithm, supereight [44], was used for integration and visualising an exemplary ScanDrone map of the print as a 3D mesh (Fig. 3). Besides in-the-loop qualitative and quantitative analyses of the built geometry, the map crucially enables adjusting the print trajectory height of the next layer (Supplementary Method 4).

With the ScanDrone informed adjustment, the reference and effective positions of the center of mass of the BuilDrone in printing the cylinder are shown in Fig. 3a with close-up views of selected layers in Fig. 3b. With trajectories of the BuilDrone logged during the actual printing tests, the absolute position errors were quantitatively evaluated, showing that the maximum horizontal and vertical absolute position errors were within 0.015 m and 0.006 m, respectively (Fig. 3c). More detailed analysis of the positioning accuracy is illustrated in Extended Data Fig. 5.

We further compared our online 3D map mesh as created by the ScanDrone to the collected 3D Faro Laser scan (Supplementary Method 4). The mesh and point-cloud were aligned manually initially and then refined by the Iterative Closest Point (ICP) algorithm using the CloudCompare tool. The analysis of point-to-triangle errors reveals a median value of 2.27 cm which suffices the required accuracy in foam printing.

Small cylinder in cementitious material Print of a smaller scale cylindrical thin wall with a Peano curve path and fine filaments less than 0.01 m in diameter was undertaken to demonstrate the novel Aerial-AM approach to high-resolution manufacturing using two BuilDrones printing with custom-engineered cementitious material in turn (Fig. 4).

Each Aerial-AM BuilDrone must extrude material within power limits and payload constraints; this required the miniaturisation of AM deposition relative to ground-based methods. A cementitious Aerial-AM material must be lightweight and less dense than traditional and ground-based AM study mortars, with higher water/binder ratios and lower fine aggregate/binder ratios required (Supplementary Method 6). Investigations included the addition of foaming agents to reduce bulk density. Rheological properties in the fresh state are of primary importance [45] and rheology modifying admixtures (RMA) can alter fresh material properties [46,47]. For AM, pseudoplastic ('shear-thinning') properties are desirable, where material viscosity and yield stress decrease (while under stress in a deposition system) and increase (once extruded) [48] by orders of magnitude. During Aerial-AM mix development, Hydroxyethyl methyl cellulose (HEMC) and xanthan gum were discovered to be synergistic and provided fresh mixes with suitable rheological properties and resistance to propeller downwash. This synthetic hygroscopic (HEMC) and natural hydrophilic (xanthan gum) polymeric hydrocolloid combination effectively resulted in a cementitious-polymeric composite material for Aerial-AM. Four novel lightweight mixes suitable for BuilDrone extrusion were developed (mixes No. 1-4, Extended Data Fig. 6) and a range of tests (Supplementary Table 5) were carried out to indicate magnitudes of material properties in fresh and cured states. Mix No.3 was used for the cementitious print, demonstrating that with the use of RMAs, fine aggregate is not essential for Aerial-AM; removing fine aggregate eliminates the need to add foam, significantly decreasing mix preparation time and increasing productivity. To summarise, a cementitious material suitable for Aerial-AM has a bulk density in the region of 1700 kg/m^3, fresh properties (within open time) with a complex modulus of 7 MPa, phase angle of 4°, yield stress of 1.1 kPa, a viscosity profile decreasing by five orders of magnitude while under stress, and a resulting cured 28-day compressive strength in the order of 25 MPa.

To manufacture geometry with high-resolution details using cementitious material, a new type of Aerial-AM BuilDrone was customised to enhance the printing accuracy by integrating a dexterous delta manipulator and moving the material deposition nozzle along with end-effector of the manipulator (Extended Data Fig. 2). With trajectory tracking data obtained during the light-trail virtual print of a thin-walled cylinder of 1.2 m in height, we evaluated the accuracy of the BuilDrone pose, as well as the tip position of the nozzle (Fig. 4a,b), in performing printing tests employing the Model Predictive Control schemes (Extended Data Fig. 4, Supplementary Method 3, Supplementary Video 4). Respective Root-Mean-Square Errors (RMSE) per layer of printing are provided (Extended Data Table 1) for both the BuilDrone position and the nozzle tip position. We further studied the BuilDrone position reference and effective position per axis (Extended Data Fig. 7). The statistical analyses of the experiments showed that the nozzle tip achieved higher accuracy than the BuilDrone itself. The results reveals that the delta manipulator can effectively compensates for deviations not only in the BuilDrone position, but also from tip shifts due to altitude deviation as a function of the lever arm between the BuilDrone's center of mass and the nozzle tip (Fig. 4c).

With the optimized cementitious mix No. *3* and high accuracy of the BuilDrones with integrated delta manipulators, printing path designs (Extended Data Fig. 3) were adapted to manufacture a cementitious thin-walled cylinder with a maximum outer diameter of 0.335 m using the deposition system with a nozzle of 8 mm in diameter (Supplementary Video 5). Using the three scalable printing paths (Extended Data Fig. 3a), material deposition tests

(Supplementary Experiment S1) indicated the rounded Peano curve design has advantages in two aspects. First, it requires less material for thin-wall cylinders with identical diameters: 5.85 m printed length per two layers compared to 6.79 m for the hybrid design and 7.61 m for the concentric circles design. Second, it maintains contact points consistent between two adjacent layers even with some deposition imprecision, with favourable aesthetic qualities. Results also indicated a favourable load per material used ratio in comparison to concentric circles.

Using two BuilDrones with integrated delta manipulators, we additively manufactured a 28-layer thin-walled cylinder (Supplementary Video 6). The speed of the BuilDrones for printing the cylinder was 10×10^{-3} m/s and the materials in the cartridge of deposition device was accordingly driven to deposit a 10×10^{-3} m bead of material per second, resulting in a flow velocity of the material of 0.294×10^{-3} m/s in the cartridge and 4.44×10^{-3} m/s in the flexible tubing of 8×10^{-3} m inner diameter. Printing velocities for the cylinder with a 6×10^{-3} m layer resolution are summarised in Extended Data Table 2.

Each layer involved the deposition of mix No.3 following the rounded Peano curve printing path, resulting in a deposition length of 2.975 m that utilised the effective capacity of each BuilDrone's material payload, and required a material refill after each layer. The thickness of each fresh layer was determined by both the circular nozzle orifice diameter (8×10^{-3} m) and the minor stretching force while the nozzle tip moves along the printing path. With 10×10^{-3} m/s printing speed, it took 2 hours 13 minutes in total for material deposition only to complete the cylinder. The final height of the 28-layered thin-walled cylinder was 180×10^{-3} m after the material settled.

Multi-robot virtual print and simulation The third experiment validates system adaptation of the Aerial-AM approach through a live flight demonstration, virtually printing a parabolic surface of revolution with varied print contour layer radii using a light-trail time-lapse (Fig. 5). Extending this result, we then simulated the behaviour of multi-robot parallel additive manufacturing across a range of geometries with increasing scale and robot population size. Highlighting the system's ability to adapt to variations in print geometry we compared results between two classes of surface revolution: cylinders with a constant radius, and a surface of revolution based on a parabolic function that consists of a decreasing print-contour area towards the end of the AM process near the top (Fig. 5). This specific surface was utilized to demonstrate a geometry where print layers near the end of the printing assignment require a different number of BuilDrones compared to lower contours of greater area; providing a scenario to evaluate scalability and adaptation in the number of robots undertaking printing in parallel, whilst also managing in-situ congestion constraints. To ensure comparability, the manufacturing print length was made equal for both geometries of equivalent base radii. Their circular footprint and radial symmetry also ensured that our experimental set-up (Supplementary Fig. 10) was consistent for all robots radially arrayed around the workspace perimeter.

We evaluated the real-world performance of the Aerial-AM framework for multi-robot flight in virtual printing a parabolic surface of revolution geometry with a base diameter of 2.5 m (Supplementary Fig. 10), using a team of 3 aerial robots converted from ScanDrones by adding an LED array per robot to signify their printing states (by colour) in lieu of a material deposition system (Fig. 5 and Supplementary Experiment S2).

The geometry was segmented into horizontal print contour layers representing a total of 176 individual Print Jobs that individual robots could adaptively select throughout the printing process (Fig. 5a,c). Indicated by the red paths plotted in Fig. 5a,c and colour-coded for each individual robot as recorded in flight data (Fig. 5b,d), local path planning solutions enabled multiple Print Jobs to be executed concurrently whilst also providing real-time features for collision awareness between the robots and virtual geometries that vary in diameter during building. The virtual print shows the framework was able to adapt to changes in contour geometry, by self-retiring the number of robots given the increasing spatial constraints associated with height (Supplementary Experiment S2). Altogether, these results highlight the ability of the Aerial-AM framework to adapt building operations relative to geometry through self-optimisation of robot path planning and congestion avoidance (Supplementary Video 7).

Informed by the the virtual print results, a set of simulation experiments were undertaken that tested variations in printing behaviour by changing the number of available robots, in addition to sizes of surface revolution geometries with both constant (cylindrical) and varying diameters (parabolic) (Supplementary Experiments S3, Supplementary Figs. 11-16). To assess the impact of a constant (cylinder) versus variable (parabolic) contour area throughout a printing assignment, the geometries tested had the same base diameters and total printing lengths. These studies demonstrated robot population size adaptation relative to changes in print contour layer area throughout the printing of each geometry (Supplementary Figs. 18,19). Increases in robot population were shown to produce a significant decrease in time to completion for each geometry. As expected, larger diameter geometries exhibited greater rates of reduction in time to completion from increases in robot population. In contrast, completion rates for parabolic geometries with varying diameters did not reduce to match cylindrical geometries' completion times due to their smaller average print contour layer area compared with geometries of the same base diameter (Supplementary Fig. 17). Distributed printing behaviours were also demonstrated, whereby robot participation numbers were able to dynamically vary based upon the available printing tasks. Fig. 5f shows the resulting print job distribution across 15 robots operating in parallel within a simulated construction of a larger 15 m diameter parabolic surface of revolution geometry. This result was comparable to similar distributed robot participation numbers as shown in the live light-trail experiments (Fig. 5b,d, Supplementary Fig. 17).

3 Discussion and Open Questions

Through actual additive manufacturing with both foam and cementitious material, virtual AM light-painting flights, and simulation experiments using varying size and print contour layer area geometries, we systematically developed the Aerial-AM framework as an autonomous, scalable and flexible approach to additive manufacturing that is adaptable to variations in geometry type, scale and robot population. Printing of the tall cylinder of 2.05 m in height using BuilDrone for material deposition and ScanDrone for in-the-loop qualitative assessment of the printed structure demonstrated the capacity of the Aerial-AM approach for manufacturing large-scale geometry. The manufacture of a cementitious thin-walled cylinder proved that the coupling of a self-aligning delta parallel manipulator to the BuilDrone allowed material deposition at high accuracy (maximum 5 mm position error) in both lateral and vertical directions, which is acceptable and within UK building requirements [49]. The virtual light-trail additive manufacturing and simulation results reveal that the Aerial-AM framework can effectively print various geometries by parallel multi-robot manufacturing while mitigating for excess congestion, and demonstrate adaptation and individual robot redundancy.

While these experiments successfully validate the feasibility of Aerial-AM, they are just the first steps in exploring the potential of using aerial robots for construction. Significant advances in robotics and material science are required to enable the full-scale manufacturing of building geometries using the proposed approaches. In particular, the deposition of support materials, active material curing, and task-sharing between multiple robots, are frontiers that need to be further developed. Further research on the design and engineering of structurally efficient geometries suited to Aerial-AM, and systematic analyses of the structural behaviour of printed geometries, is required. Our parallel investigations in this area suggest there are geometries that could successfully leverage Aerial-AM capabilities [50].

In order to take the research outside the confines of the indoor lab, we intend to implement a multi-sensor SLAM system with Differential GPS to provide adequate outdoor localization. Scaling up of the manufacturing volume will require automation of material and battery replenishment, while further means of assessment are needed to evaluate the efficiency of distributed manufacturing relative to the scale of the manufactured object and the robot platforms used.

However, the system presented here demonstrates a proof of concept for autonomous Aerial-AM, and may serve to provide a foundation for realising construction using collective multi-robot additive manufacturing systems. With continued development, Aerial-AM could provide an alternative means to support housing and vital infrastructure in remote locations, where the impact of global warming and unprecedented increases in the frequency of natural disasters and the hostility of climatic conditions render existing approaches to building challenging.

References

1. Lim, S., Buswell, R., Le, T., Austin, S., Gibb, A. & Thorpe, T. Developments in construction-scale additive manufacturing processes. *Automation In Construction.* **21**, 262-268 (2012)

2. Gosselin, C., Duballet, R., Roux, P., Gaudilliere, N., Dirrenberger, J. & Morel, P. Large-scale 3D printing of ultra-high performance concrete–a new processing route for architects and builders. *Materials And Design.* **100**, 102-109 (2016)

3. Keating, S., Leland, J., Cai, L. & Oxman, N. Toward site-specific and self-sufficient robotic fabrication on architectural scales. *Science Robotics.* **2**, 15 (2017)

4. Buswell, R., Silva, W., Jones, S. & Dirrenberger, J. 3D printing using concrete extrusion: A roadmap for research. *Cement And Concrete Research.* (2018)

5. The 21st century revolution in building technology has a name. $https://www.cadblog.pl/podcasty/luty_2012/d_shape_presentation.pdf$ (2009)

6. BigDelta WASP 12m. $https://www.3dwasp.com/en/giant-3d-printer-bigdelta-wasp-12mt$(2016)

7. Butters, D., Sustarevas, J., Hammid, M., Pawar, V., Dwyer, G. & Stuart-Smith, R. MAP - A Mobile Agile Printer Robot for on-site Construction. (Institute of Electrical,2019)

8. Zhang, X., Li, M., Lim, J., Weng, Y., Tay, Y., Pham, H. & Pham, Q. Large-scale 3D printing by a team of mobile robots. *Automation In Construction.* (2018)

9. Off-site manufacture for construction: Building for change. https://publications.parliament.uk/pa/ld201719/ldselect/ldsctech/169/16902.htm (2018)

10. Khoshnevis, B. Automated construction by contour crafting related robotics and information technologies. *Automation In Construction.* **13**, 5-19 (2004)

11. Hansell, M. Built by animals: the natural history of animal architecture. (OUP Oxford,2007)

12. Theraulaz, G., Bonabeau, E. & Deneubourg, J. The mechanisms and rules of coordinated building in social insects. *Information Processing In Social Insects.* 309-330 (1999)

13. Petersen, K., Napp, N., Stuart-Smith, R., Rus, D. & Kovac, M. A review of collective robotic construction. *Science Robotics.* **4** (2019)

14. Delgado, J., Oyedele, L., Ajayi, A., Akanbi, L., Akinade, O., Bilal, M. & Owolabi, H. Robotics and automated systems in construction: Understanding industry-specific challenges for adoption. *Journal Of Building Engineering.* **26**, 100868 (2019)

15. Tay, Y., Panda, B., Paul, S., Noor Mohamed, N., Tan, M. & Leong, K. 3D printing trends in building and construction industry: a review. *Virtual And Physical Prototyping.* **12**, 261-276 (2017)

16. Lindsey, Q., Mellinger, D. & Kumar, V. Construction of Cubic Structures with Quadrotor Teams. *Robotics: Science And Systems VII.* (2011)

17. Mirjan, A., Augugliaro, F., D'Andrea, R., Gramazio, F. & Kohler, M. Building a bridge with flying robots. *Robotic Fabrication In Architecture, Art And Design 2016.* 34-47 (2016)

18. Stuart-Smith, R. Behavioural Production: Autonomous Swarm-Constructed Architecture. *Architectural Design*. **86**, 54-59 (2016)

19. Furrer, F., Wermelinger, M., Yoshida, H., Gramazio, F., Kohler, M., Siegwart, R. & Hutter, M. Autonomous robotic stone stacking with misc next best object target pose planning. *2017 IEEE International Conference On Robotics And Automation (ICRA)*. 2350-2356 (2017)

20. Kayser, M., Cai, L., Falcone, S., Bader, C., Inglessis, N., Darweesh, B. & Oxman, N. Design of a multi-agent, fiber composite digital fabrication system. *Science Robotics*. **3**, eaau5630 (2018)

21. Hutter, M., Diethelm, R., Bachmann, S., Fankhauser, P., Gehring, C., Tsounis, V., Lauber, A., Guenther, F., Bjelonic, M., Isler, L. & Others Towards a generic solution for inspection of industrial sites. *Field And Service Robotics*. 575-589 (2018)

22. Chermprayong, P., Zhang, K., Xiao, F. & Kovac, M. An integrated delta manipulator for aerial repair: A new aerial robotic system. *IEEE Robotics and Automation Magazine*. **26**, 54-66 (2019)

23. Bellingham, J. & Rajan, K. Robotics in remote and hostile environments. *Science*. **318**, 1098-1102 (2007)

24. Helm, V., Ercan, S., Gramazio, F. & Kohler, M. Mobile robotic fabrication on construction sites: DimRob. *Intelligent Robots And Systems (IROS), 2012 IEEE/RSJ International Conference On*. 4335-4341 (2012)

25. Werfel, J., Petersen, K. & Nagpal, R. Designing collective behavior in a termite-inspired robot construction team.. *Science (New York, N.Y.)*. **343**, 754-8 (2014)

26. Willmann, J., Augugliaro, F., Cadalbert, T., D Andrea, R., Gramazio, F. & Kohler, M. Aerial robotic construction towards a new field of architectural research. *International Journal Of Architectural Computing*. **10**, 439-459 (2012)

27. Augugliaro, F., Lupashin, S., Hamer, M., Male, C., Hehn, M., Mueller, M., Willmann, J., Gramazio, F., Kohler, M. & D'Andrea, R. The flight assembled architecture installation: Cooperative construction with flying machines. *IEEE Control Systems Magazine*. **34**, 46-64 (2014)

28. MINIBUILDERS. $https://iaac.net/project/minibuilders/$ (2016)

29. Speich, S., Jones, H. & Benedict, E. Review of the natural nesting of the Barn Swallow in North America. *American Midland Naturalist*. 248-254 (1986)

30. Miriyev, A. & Kovač, M. Skills for physical artificial intelligence. *Nature Machine Intelligence*. **2**, 658-660 (2020)

31. Zareiyan, B. & Khoshnevis, B. Interlayer adhesion and strength of structures in Contour Crafting-Effects of aggregate size, extrusion rate, and layer thickness. *Automation In Construction*. **81**, 112-121 (2017)

32. Zareiyan, B. & Khoshnevis, B. Effects of mixture ingredients on interlayer adhesion of concrete in Contour Crafting. *Rapid Prototyping Journal*. (2018)

33. Le, T., Austin, S., Lim, S., Buswell, R., Gibb, A. & Thorpe, T. Mix design and fresh properties for high-performance printing concrete. *Materials And Structures.* **45**, 1221-1232 (2012)

34. Wangler, T., Lloret, E., Reiter, L., Hack, N., Gramazio, F., Kohler, M., Bernhard, M., Dillenburger, B., Buchli, J., Roussel, N. & Others Digital concrete: opportunities and challenges. *RILEM Technical Letters.* **1**, 67-75 (2016)

35. Lloret Fritschi, E. Smart Dynamic Casting-A digital fabrication method for non-standard concrete structures. (ETH Zurich,2016)

36. Hack, N., Wangler, T., Mata-Falcón, J., Dörfler, K., Kumar, N., Walzer, A., Graser, K., Reiter, L., Richner, H., Buchli, J. & Others Mesh mould: an on site, robotically fabricated, functional formwork. *Second Concrete Innovation Conference (2nd CIC), Paper.* (2017)

37. Bos, F., Wolfs, R., Ahmed, Z. & Salet, T. Additive manufacturing of concrete in construction: potentials and challenges of 3D concrete printing. *Virtual And Physical Prototyping.* **11**, 209-225 (2016)

38. Bos, F., Ahmed, Z., Jutinov, E. & Salet, T. Experimental exploration of metal cable as reinforcement in 3D printed concrete. *Materials.* **10**, 1314 (2017)

39. Wolfs, R., Bos, F. & Salet, T. Early age mechanical behaviour of 3D printed concrete: Numerical modelling and experimental testing. *Cement And Concrete Research.* **106**, 103-116 (2018)

40. Ghaffar, S., Corker, J. & Fan, M. Additive manufacturing technology and its implementation in construction as an eco-innovative solution. *Automation In Construction.* **93**, 1-11 (2018)

41. Barnett, E. & Gosselin, C. Large-scale 3D printing with a cable-suspended robot. *Additive Manufacturing.* **7**, 27-44 (2015)

42. Subrin, K., Bressac, T., Garnier, S., Ambiehl, A., Paquet, E. & Furet, B. Improvement of the mobile robot location dedicated for habitable house construction by 3D printing. *IFAC-Papersmisc.* **51**, 716-721 (2018)

43. Marchon, D., Kawashima, S., Bessaies-Bey, H., Mantellato, S. & Ng, S. Hydration and rheology control of concrete for digital fabrication: Potential admixtures and cement chemistry. *Cement And Concrete Research.* **112**, 96-110 (2018)

44. Vespa, E., Funk, N., Kelly, P. & Leutenegger, S. Adaptive-resolution octree-based volumetric SLAM. *2019 International Conference On 3D Vision (3DV).* 654-662 (2019)

45. Jiao, D., Shi, C., Yuan, Q., An, X., Liu, Y. & Li, H. Effect of constituents on rheological properties of fresh concrete-A review. *Cement And Concrete Composites.* **83**, 146-159 (2017)

46. Lootens, D., Hébraud, P., Lécolier, E. & Van Damme, H. Gelation, shear-thinning and shear-thickening in cement slurries. *Oil and Gas Science And Technology.* **59**, 31-40 (2004)

47. Studart, A. Additive manufacturing of biologically-inspired materials. *Chemical Society Reviews.* **45**, 359-376 (2016)

48. Chen, M., Li, L., Zheng, Y., Zhao, P., Lu, L. & Cheng, X. Rheological and mechanical properties of admixtures modified 3D printing sulphoaluminate cementitious materials. *Construction And Building Materials.* **189**, 601-611 (2018)

49. Group, C. National structural concrete specification for building construction. (Crowthorne: British Cement Association,2000)

50. Ander, M., Olsson, J., Shepherd, P., Stuart-Smith, R. & Williams, C. A building of unlimited height. *Proceedings Of IASS Annual Symposia.* **2019**, 1465-1472 (2019)

FIGURE LEGENDS:

Figure 1: Additive Manufacturing in the building industry. Comparison of different additive manufacturing robot platforms. Established platforms exhibit limitations in scale of additive manufacturing job vs scale of robot platform, maximum build envelope, ability to manufacture in parallel, and site access capabilities. Aerial-AM enables parallel manufacturing with an unbounded build envelope in hard-to-access locations.

Figure 2: The Aerial-AM framework for untethered and unbounded additive manufacturing. **a**, The proposed multi-agent aerial-AM framework consists of two loops that operate at a strategic slow and a real-time operational fast time-scale for manufacturing and progress observation. **b**, Print of a proof of concept large-scale cylindrical geometry

using a BuilDrone that additively manufactures an expansion foam material and a ScanDrone that 3D scans the manufactured geometry utilizing an on-board vision system for progress mapping. The print demonstrates a faster build rate and large-scale geometry using the foam material. **c**, Experimental printing demonstration involving two BuilDrones that additively manufacture 28 layers of cementitious material by sequentially flying between a ground station and the additive manufacturing site. Here materials deposition relies on the high accuracy of BuilDrones enabled by an onboard error compensating delta manipulator in the experimental space with accurate state estimation. **d**, Virtual manufacture and simulation of a surface of revolution based on a parabolic profile with the base diameter of 2.5 m using 3 and more printing robots.

Figure 3: A tall cylindrical geometry of 2.05 m in height printed with 72 material deposition trips by a Aerial-AM BuilDrone and real-time print evaluation by a ScanDrone. **a**, The trajectories of the centre of mass of the BuilDrone, with position reference (in red) and actual position (in blue), during the foam printing using a scalable circle path design. **b**, The close-up view of the reference circle path and the actual position for the printing of layers 10, 36, and 72. **c**, Mesh reconstructions from ScanDrone, including top-view heatmap used for automatic height adjustment at layers 10, 36 (half height) and perspective side-views at layers 10, 36 and 72 (full height) of the foam cylinder. **d**, Position accuracy of the BuilDrone tracing the designed reference circular trajectory, showing the horizontal and vertical absolute position errors with median error values of 1.5 cm and 0.6 cm, respectively.

Figure 4: 3D printing a thin-walled cylinder by two BuilDrones with error compensating delta manipulator depositing cementitious material. **a**, BuilDrones' position reference (in red) and actual position of fixed depositing nozzle tip (in blue) during the virtual printing of a meter-scale cylinder using the rounded Peano curve path design. **b**, The close-up view of the reference rounded Peano curve path and the actual tip position for tests with a compensation function from the delta parallel manipulator and tests without the compensation function. It illustrates the function of the integrated delta parallel manipulator for achieving higher accuracy at the tip of the deposition nozzle which is positioned a distance away from the mass center of the BuilDrone. **c**, Quantitative evaluation of position accuracy of the tip of depositing nozzle at two different printing speeds. In the virtual printing tests at 5 cm/s printing speed, the absolute position error in the lateral direction is higher than 0.5 cm, which may be caused by the trajectory geometry's small curvatures being difficult to implementing at an increased flight speed. In the real tests at 1 cm/s printing speed, the median value of absolute horizontal position error is less than 0.4 cm which was acceptable for the 0.8 cm diameter nozzle. **d**, Printing progress of the cylinder (front view) using two BuilDrones working in sequence, including the layers of 1, 10, 19 and 28.

Figure 5: Aerial-AM multi-robot light-trail virtual print of a surface of revolution embodying a varying radius. **a**, Light-trail time-lapse mid-construction: red paths indicating trajectories when robot is not printing, blue paths highlight paths in which the robot would be printing. **b**, Top view and **d**, perspective view of the light-trail flight trajectory analysis of flight with 3 robots, where colours identify individual robots'

completed print job tasks. **c**, Light-trail time-lapse of the complete geometry. **e**, Overlay of robot starting positions when not printing (red light) and printing (blue light). **f**, Simulation results with 15 drones printing a scaled up version of the geometry measuring 15 m in base diameter.

Acknowledgements We would like to acknowledge the support of the Engineering and Physical Sciences Research Council (EPSRC) awards under grant agreements EP/N018494/1, EP/K005030/1 and EP/S031464/1, EPSRC Centre for Decarbonisation of the Built Environment (dCarb) under grant agreement EP/L016869/1, the Royal Society Wolfson Fellowship under grant number RSWFR1180003 (M. Kovac), the Royal Thai Government Scholarship (P. Chermprayong), the University of Bath Research Scholarship (B. Dams), and the Department of Aeronautics of Imperial College London. We also thank Dr. Talib Al-Hinai and Dr Robert Siddall for their contributions in the early conceptualization stage of the project, and Mr. Zhujin Jiang and Mr. Chen Liu for their assistance in experimental tests and multi-media files preparation.

Author contributions K.Z., S.S., L.M., V.M.P., R.J.B., C.W., P.S., S.L., R.S.-S. and M.K. conceived the study. K.Z., P.C., B.K., L.O. and M.K. designed and engineered the Aerial-AM robots and material extrusion system. D.T., W.L., C.C., P.C., K.Z., M.K. and S.L. designed and analysed the controller for the Aerial-AM robots. B.D., S.A.N., and R.B. engineered the material mixtures and performed material tests. S.K., V.M.P, S.H, K.Z., P.C., F.X., D.T., S.L. M.K and R.S.-S. designed the multi-agent framework and performed the light-trace virtual AM demonstration and simulations. C.W., P.S. and R.S.-S. performed design of proof of concept geometries. K.Z., P.C., F.X., D.T., B.D., S.K., B.K., A.B., D.D., A.C., L.M., V.M.P., S.L. and M.K. carried out system integration and Aerial-AM printing experiments with the robots. K.Z., B.D., V.M.P., L.S., R.S.-S. and M.K. wrote the manuscript. M.K and R.S.-S. conducted pilot research and initiated the research. All authors contributed to and approved the final draft of the manuscript.

Extended Data Available in the main paper and the supplementary information.

Data Availability The authors declare that the data supporting the findings of this study are available within the paper and its Supplementary Information. Each data point corresponding to figures that describe the results from experimental and simulation studies are provided as separate Source Data for Figs. 3a, b, d, 4a-c and Extended Data Figs. 5a, b, 6b-d, 7a-d. Other source data related to the study are available from the corresponding author upon reasonable request.

Code availability The custom code for all algorithm developed in this work are available from the corresponding author on reasonable request.

Supplementary information Available in an individual file.

Competing Interests The authors declare that they have no competing financial interests.

Correspondence Correspondence and requests for materials should be addressed to Dr Mirko Kovac (email: m.kovac@imperial.ac.uk).

EXTENDED DATA FIGURE LEGENDS:

Extended Data Figure 1. Aerial-AM robots. a, The BuilDrone for foam printing. The foam material canisters which store the dual components of the expansion foam are mounted underneath the quadrotor platform. The nozzle for spraying the foam material is then fixed to the bottom of the canister holder. **b**, The BuilDrone for cementitious material print. The cementitious material extruder is placed in the holder underneath the wheelbase of the BuilDrone while the upper platform of delta parallel manipulator is attached to the holder. The nozzle is mounted on the end-effector of the delta manipulator and connected to the extruder though tubing. (d: distance from nozzle to the substrate; h: single layer height; w: layer width.) **c**, The ScanDrone with an integrated RGB-D camera for 3D mapping of the printed structure.

Extended Data Figure 2. Deviation compensating using delta manipulator. **a**, The setting of BuilDrone with upper platform of delta parallel manipulator mounted underneath the quadrotor platform. **b**, Kinematic diagram of the light-weight delta parallel manipulator which has three limbs with identical kinematic structure. The end-effector with geometric center O_e implements pure translational motion with respect to the upper platform with geometric center O_c. **c**, Schematic diagram of the deviation compensation principle: the nozzle tip F keeps at desired position though the BuilDrone platform may drift to the pose at O_b' away from the reference pose at O_b. This method results in higher positional accuracy of the nozzle tip for depositing the material at target position T.

Extended Data Figure 3. Geometry designs and printed layer/s of sample printing path for thin-walled cylinders. **a**, The printing path with four concentric circles (Separation: 8 $\times 10^{-3}$ m, inner diameter (ID): 272 $\times 10^{-3}$ m, outer diameter (OD):

320×10^{-3} m). **b**, The printing path with rounded Peano curve (ID: 260×10^{-3} m, OD: 320×10^{-3} m, Period of pattern: 50×10^{-3} m, Amplitude of pattern: 30×10^{-3} m, Closest approach between successive shapes: 8×10^{-3} m. **c**, The hybrid printing path including concentric circles and compact rounded Peano curve in alternative layers (ID: 255×10^{-3} m, OD: 335×10^{-3} m, Straight lines separation: 20×10^{-3} m, Sinusoidal period: 18×10^{-3} m, Sinusoidal amplitude: 52×10^{-3} m). **d**, The first layer of a printed sample using pure concentric circles. **e**, The first layer and the half-unit offset second layer of a printed sample using rounded Peano curve printing path. **f**, The first two layers printed using the hybrid printing path. **g-i**, The top view of the printed samples with 5 layers using three different path designs respectively. **j-l**, Front view of the five-layer structures.

Extended Data Figure 4. Robot Operating System (ROS) based control architecture for Aerial-AM robot platforms. **a**, High-level control architecture. **b**, Model Predictive Control diagram for trajectory tracking for both BuilDrone and ScanDrone. **c**, Control architecture of BuilDrone deviation compensation using the integrated delta manipulator.

Extended Data Figure 5. Position errors of the BuilDrone platform during the foam printing in flight. **a**, BuilDrone position error measured using the centre of mass. **b**, Absolute position error of the centre of mass of BuilDrone.

Extended Data Figure 6. The four cementitious-polymeric composite mixes trialled with the BuilDrone. *No.1* (green), *No.2* (orange), *No.3* (red) and *No.4* (blue), with mix *No.1* possessing the best buildability (the ability of the material to retain shape and resist deformation following extrusion due to subsequently deposited layers) and mix *No.4* the best workability (the ability of a material to be pushed through and extruded from a deposition device). **a**: Potential constituents plotted to show contribution to the properties of mixes. Workability was considered to be the primary parameter, with the selected constituents for mix formulation highlighted. **b**: The full constituent specifications of mixes *No.1*-*No.4* in kg/m^3 to three significant figures. *Key*: CEM1=Portland Cement, PFA=Pulverised Fuel Ash, Xan=Xanthan gum, hemc=Hydroxyethyl methyl cellulose, Foam=EAB Associates foaming agent mixed with water and brought to a stiff-peak consistency, Plast.=Adoflow 'S' plasticiser. Fresh mix densities: *No.1*: 1793 kg/m^3, *No.2*: 1741 kg/m^3, *No.3*: 1757 kg/m^3 *No.4*: 1760 kg/m^3. **c**: Viscosity flow profiles for mixes *No.1*-*No.4* and viscosity values relating to the four mixes while at rest, in the cartridge vessel and in the tubing indicated. **d**: Selected material parameters giving an overview of cementitious mix properties *No.1*-*No.4*. *Key*: phase angle δ (°), complex modulus $G*$, 28-day compressive strength f_{28c}, 28-day flexural strength f_{28f} (all MPa) and the force required to process the material through the deposition device and tubing (N), the value shown on the figure being the true value divided by a factor of 10. For purposes of clarity and presentation, error bars for the individual material properties are included in the respective cementitious materials test sections and the table (Supplementary Table 5) providing an summary of tests in Supplementary Experiment S1, which also contains information on sample size and additional material parameters including yield stress, which ranged from 0.7 (Mix 4) to 1.1 kPa (Mixes 1-3).

Extended Data Figure 7. Position errors of the BuilDrone platform and the printing nozzle tip during the cementicious material printing in flight. **a**, BuilDrone position error. **b**, Position error of the tip of depositing nozzle mounted on delta manipulator's end-effector. During the print, the tubing was filled with material and becomes stiffer. This led to negative errors in x- and y-direction. **c**, BuilDrone absolute position error. **d**, Absolute position error of the tip of the depositing nozzle.

EXTENDED DATA TABLE LEGENDS:

Extended Data Table 1. RMSE per layer for BuilDrone position and depositing nozzle tip position.

Extended Data Table 2. Aerial-AM BuilDrone cementitious material deposition system printing velocities.

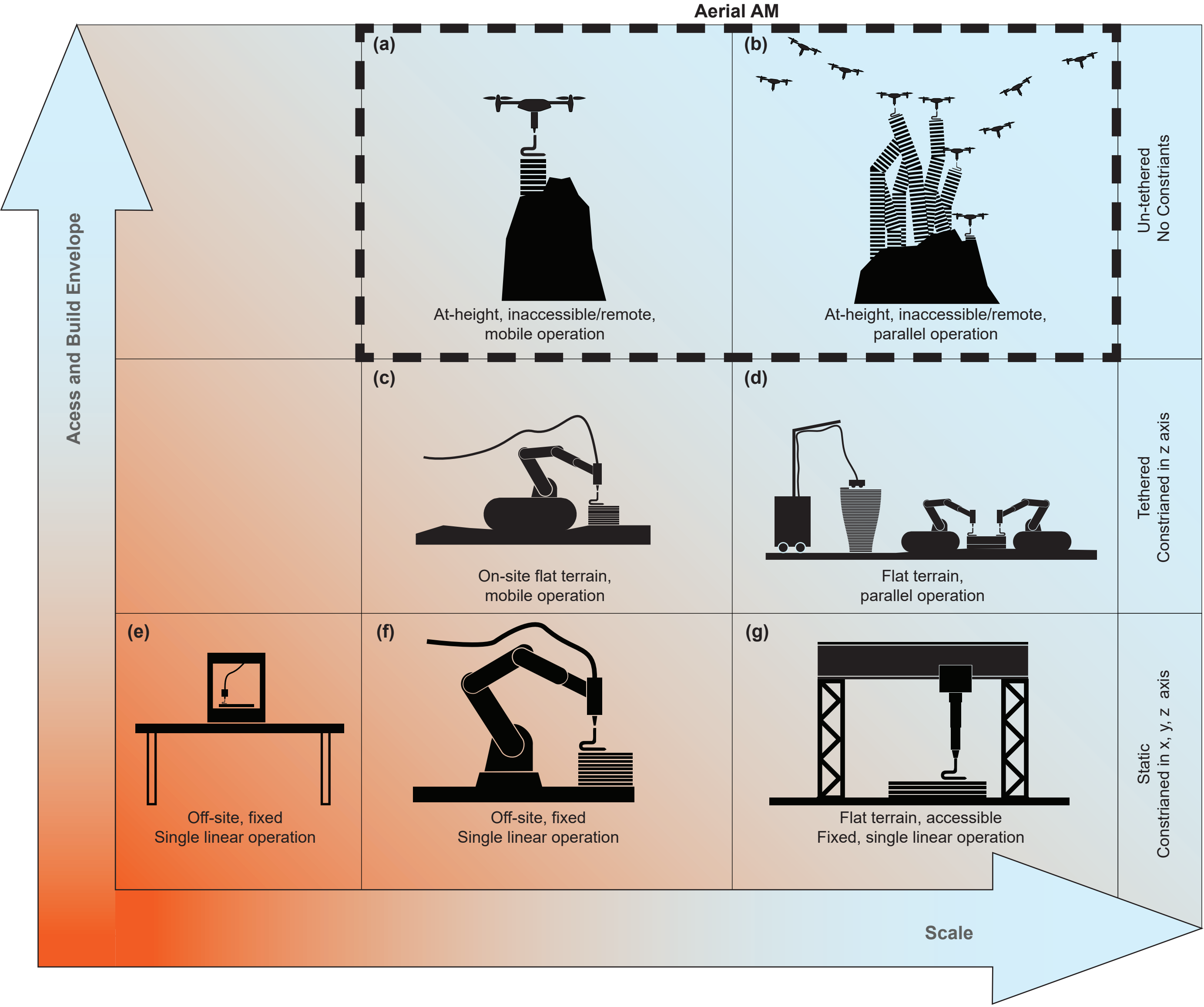
Aerial AM
(a)
At-height, inaccessible/remote, mobile operation
(b)
At-height, inaccessible/remote, parallel operation
Un-tethered
No Constriants
(c)
On-site flat terrain, mobile operation
(d)
Flat terrain, parallel operation
Tethered
Constrianed in z axis
(e)
Off-site, fixed
Single linear operation
(f)
Off-site, fixed
Single linear operation
(g)
Flat terrain, accessible
Fixed, single linear operation
Static
Constrianed in x, y, z axis
Acess and Build Envelope
Scale

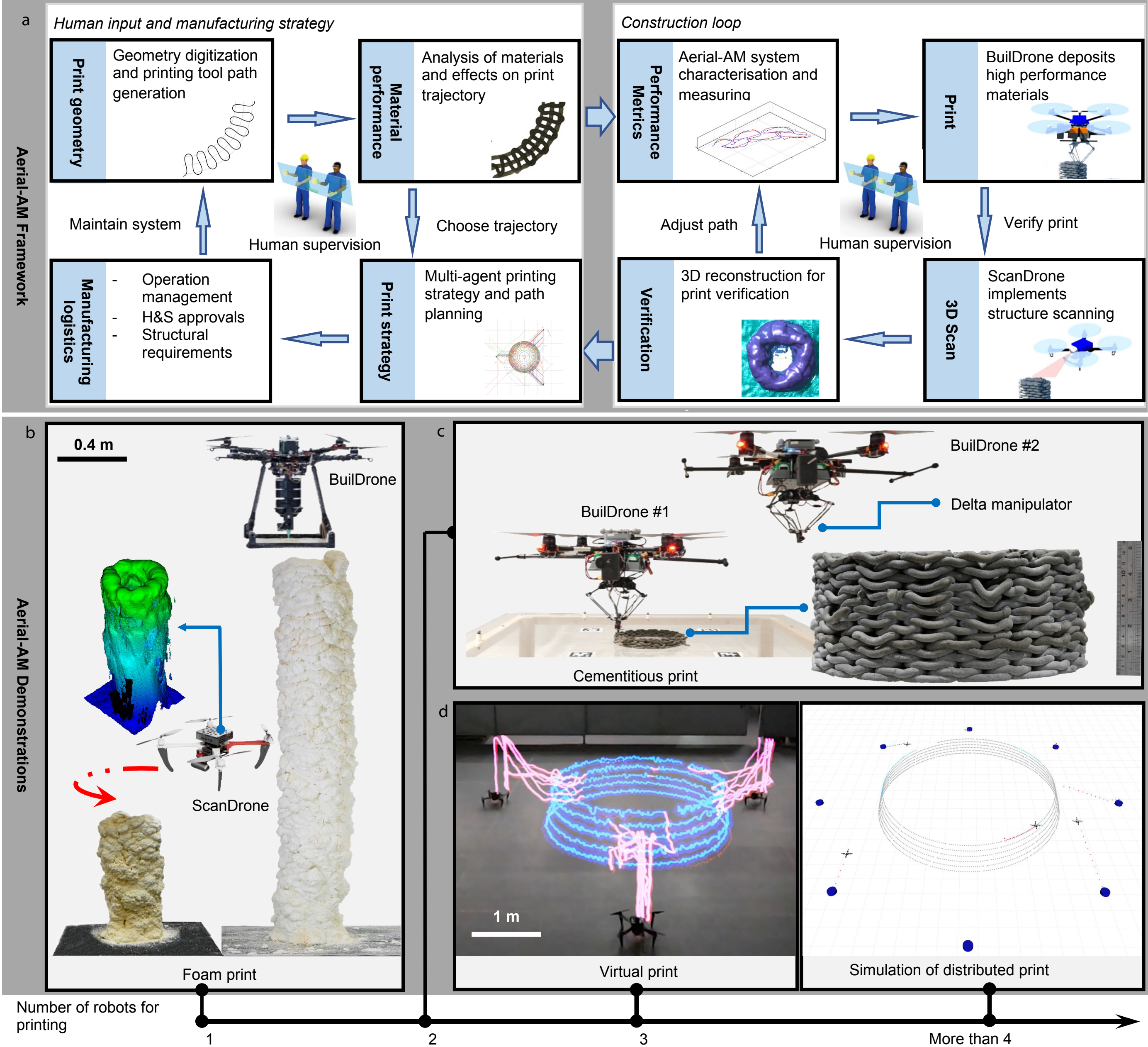
a
Aerial-AM Framework
Human input and manufacturing strategy
Print geometry
Geometry digitization and printing tool path generation
Material performance
Analysis of materials and effects on print trajectory
Maintain system
Human supervision
Choose trajectory
Manufacturing logistics
- Operation management
- H&S approvals
- Structural requirements
Print strategy
Multi-agent printing strategy and path planning
Construction loop
Performance Metrics
Aerial-AM system characterisation and measuring
Print
BuilDrone deposits high performance materials
Adjust path
Human supervision
Verify print
Verification
3D reconstruction for print verification
3D Scan
ScanDrone implements structure scanning
b
Aerial-AM Demonstrations
0.4 m
BuilDrone
ScanDrone
Foam print
c
BuilDrone #2
Delta manipulator
BuilDrone #1
Cementitious print
d
1 m
Virtual print
Simulation of distributed print
Number of robots for printing
1
2
3
More than 4

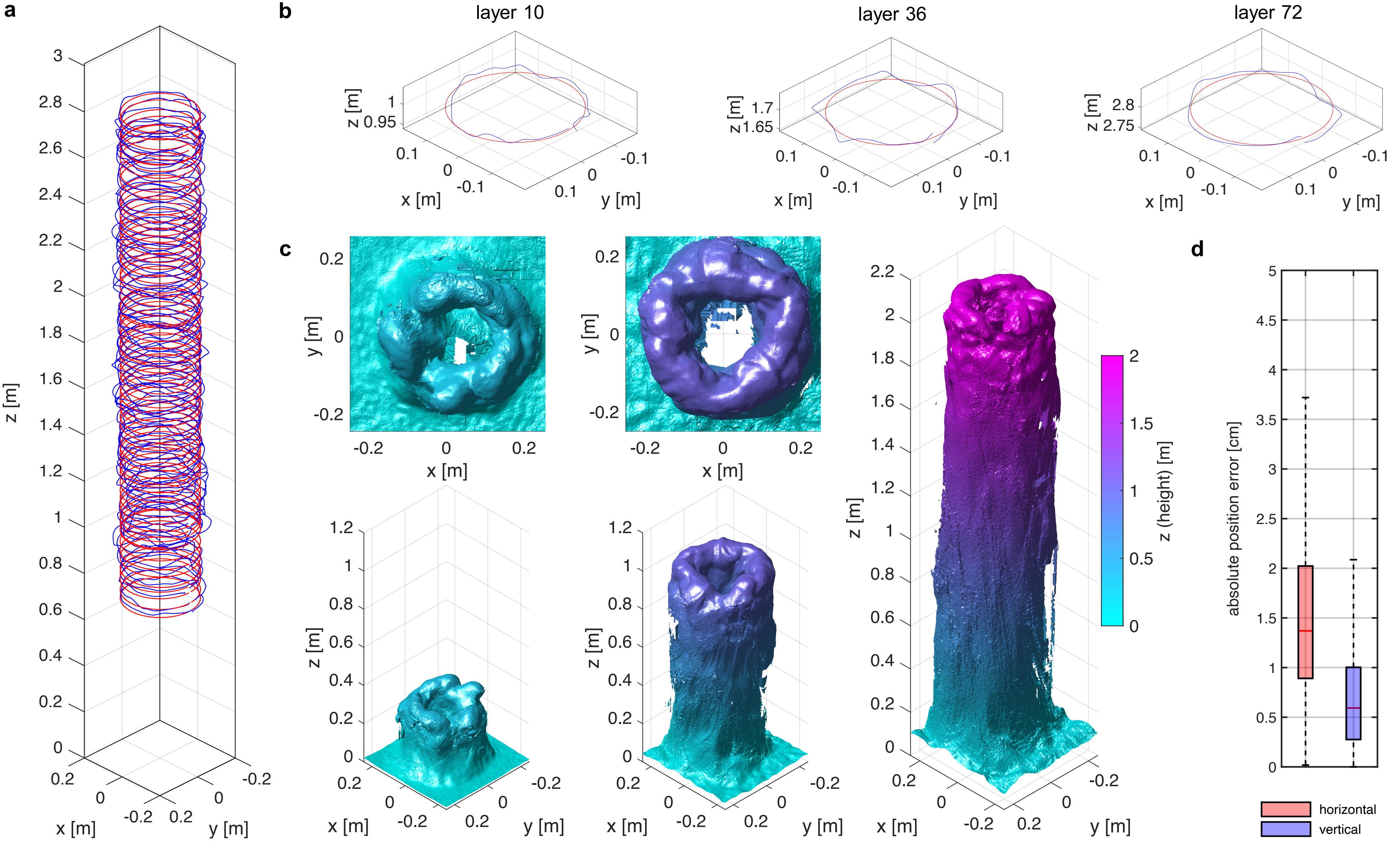
a
3
2.8
2.6
2.4
2.2
2
1.8
1.6
1.4
1.2
1
0.8
0.6
0.4
0.2
0
z [m]
0.2
0
-0.2
x [m]
0.2
0
-0.2
y [m]
b
layer 10
z [m]
1
0.95
0.1
0
-0.1
x [m]
0.1
0
-0.1
y [m]
layer 36
z [m]
1.7
1.65
0.1
0
-0.1
x [m]
0.1
0
-0.1
y [m]
layer 72
z [m]
2.8
2.75
0.1
0
-0.1
x [m]
0.1
0
-0.1
y [m]
c
0.2
y [m]
0
-0.2
-0.2
0
0.2
x [m]
0.2
y [m]
0
-0.2
-0.2
0
0.2
x [m]
1.2
1
0.8
z [m]
0.6
0.4
0.2
0
0.2
0
-0.2
x [m]
0.2
0
-0.2
y [m]
1.2
1
0.8
z [m]
0.6
0.4
0.2
0
0.2
0
-0.2
x [m]
0.2
0
-0.2
y [m]
2.2
2
1.8
1.6
1.4
1.2
z [m]
1
0.8
0.6
0.4
0.2
0
0.2
0
-0.2
x [m]
0.2
0
-0.2
y [m]
2
1.5
1
0.5
0
z (height) [m]
d
5
4.5
4
3.5
3
2.5
2
1.5
1
0.5
0
absolute position error [cm]
horizontal
vertical

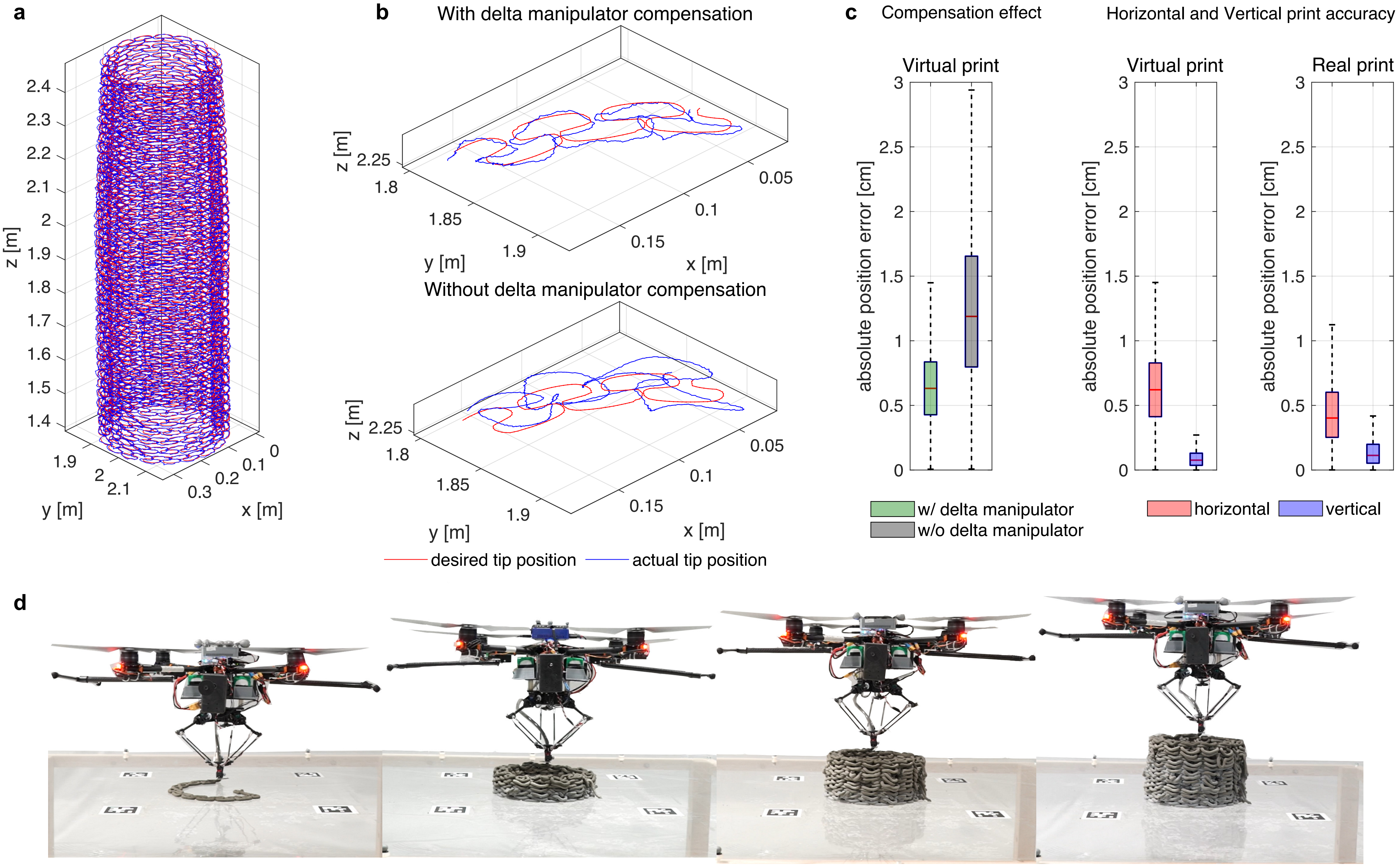
a
z [m]
2.4
2.3
2.2
2.1
2
1.9
1.8
1.7
1.6
1.5
1.4
1.9
2
2.1
y [m]
0
0.1
0.2
0.3
x [m]
b
With delta manipulator compensation
z [m]
2.25
1.8
1.85
1.9
y [m]
0.05
0.1
0.15
x [m]
Without delta manipulator compensation
z [m]
2.25
1.8
1.85
1.9
y [m]
0.05
0.1
0.15
x [m]
desired tip position
actual tip position
c
Compensation effect
Horizontal and Vertical print accuracy
Virtual print
Virtual print
Real print
absolute position error [cm]
0
0.5
1
1.5
2
2.5
3
w/ delta manipulator
w/o delta manipulator
horizontal
vertical
d

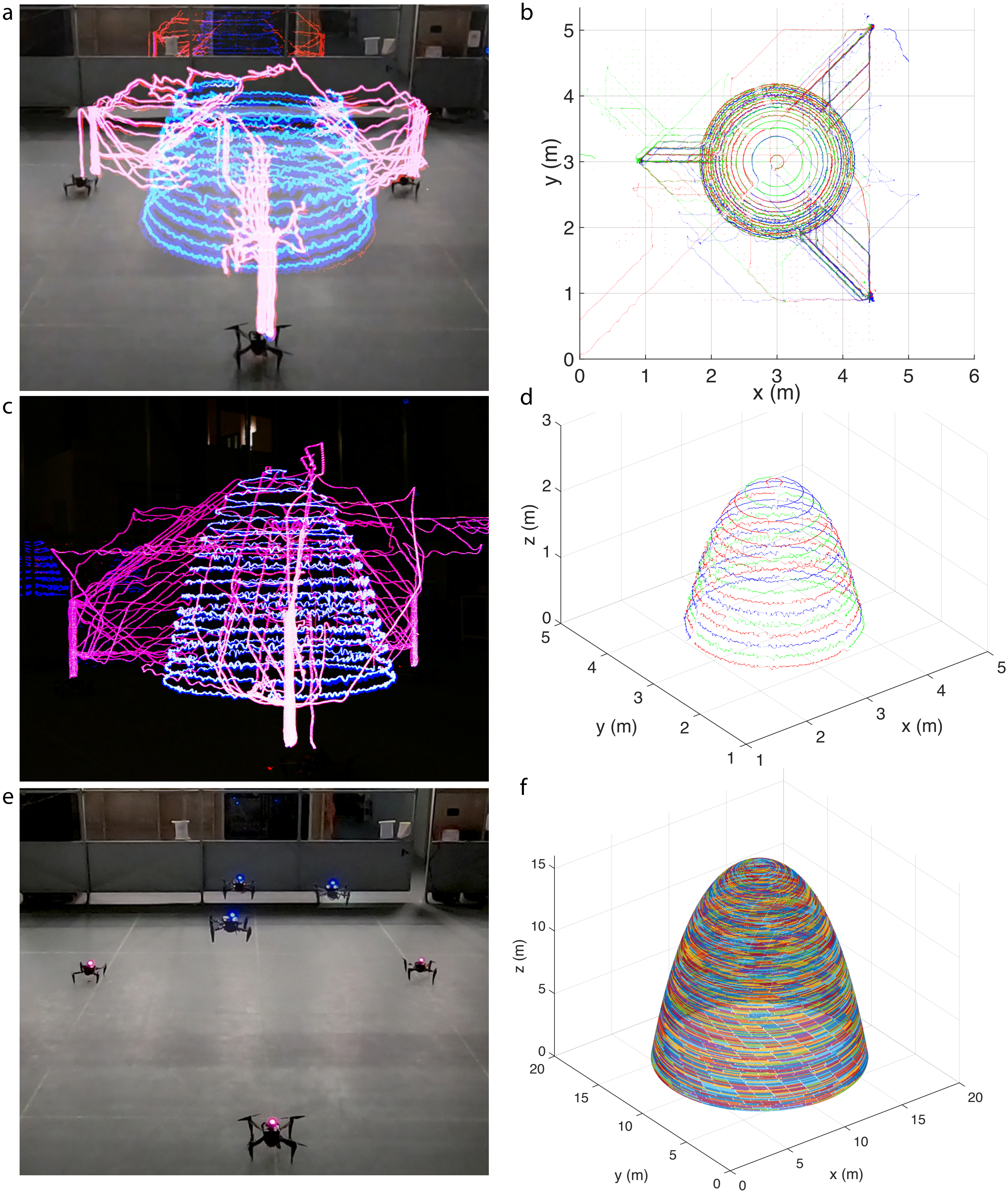
a
b
y (m)
x (m)
0
1
2
3
4
5
6
c
d
z (m)
y (m)
x (m)
e
f
z (m)
y (m)
x (m)
0
5
10
15
20